SPATIAL ACCURACY OF UAV-DERIVED ORTHOIMAGERY AND TOPOGRAPHY: COMPARING PHOTOGRAMMETRIC MODELS PROCESSED WITH DIRECT GEO-REFERENCING AND GROUND CONTROL POINTS

Chris Hugenholtz[1], Owen Brown[2], Jordan Walker[2], Thomas Barchyn[1], Paul Nesbit[1], Maja Kucharczyk[1], Steve Myshak[2]

[1]Department of Geography, University of Calgary, Calgary, Alberta, Canada

[2]Ventus Geospatial, Lethbridge, Alberta, Canada

Mapping with unmanned aerial vehicles (UAVs) typically involves the deployment of ground control points (GCPs) to georeference the images and topographic model. An alternative approach is direct georeferencing, whereby the onboard Global Navigation Satellite System (GNSS) and inertial measurement unit are used without GCPs to locate and orient the data. This study compares the spatial accuracy of these approaches using two nearly identical UAVs. The onboard GNSS is the one difference between them, as one vehicle uses a survey-grade GNSS/RTK receiver (RTK UAV), while the other uses a lower-grade GPS receiver (non-RTK UAV). Field testing was performed at a gravel pit, with all ground measurements and aerial surveying completed on the same day. Three sets of orthoimages and DSMs were produced for comparing spatial accuracies: two sets were created by direct georeferencing images from the RTK UAV and non-RTK UAV and one set was created by using GCPs during the external orientation of the non-RTK UAV images. Spatial accuracy was determined from the horizontal (X,Y) and vertical (Z) residuals and root-mean-square-errors (RMSE) relative to 17 horizontal and 180 vertical check points measured with a GNSS/RTK base station and rover. For the two direct georeferencing datasets, the horizontal and vertical accuracy improved substantially with the survey-grade GNSS/RTK receiver onboard the RTK UAV, effectively reducing the RMSE values in X, Y and Z by 1 to 2 orders of magnitude compared to the lower grade GPS receiver onboard the non-RTK UAV. Importantly, the horizontal accuracy of the RTK UAV data processed via direct georeferencing was equivalent to the horizontal accuracy of the non-RTK UAV data processed with GCPs, but the vertical error of the DSM from the RTK UAV data was 2 to 3 times greater than the DSM from the non-RTK data with GCPs. Overall, results suggest that direct georeferencing with the RTK UAV can achieve horizontal accuracy comparable to that obtained with a network of GCPs, but for topographic measurements requiring the highest achievable accuracy, researchers and practitioners should use GCPs.

La cartographie avec des véhicules aériens sans pilote (UAV) nécessite habituellement le déploiement de points d'appui au sol (GCP) pour géoréférencer les images et le modèle topographique. La géolocalisation directe est une approche de remplacement, où le Système de positionnement par satellites (GNSS) et l'unité de mesure inertielle à bord sont utilisés sans GCP pour localiser et orienter les données. Le présent article compare la précision spatiale de ces approches en utilisant deux UAV pratiquement identiques. Le GNSS embarqué est la seule différence entre eux puisqu'un véhicule utilise un récepteur GNSS/RTK de haute précision (UAV RTK) alors que l'autre utilise un récepteur GPS de précision inférieure (UAV non RTK). Un essai sur le terrain a été réalisé dans une carrière de gravier au cours duquel toutes les mesures au sol et tous les levés aériens ont été effectués le même jour. Trois séries d'orthoimages et de modèles numériques de surface (DSM) ont été produits pour comparer les précisions spatiales : deux séries ont été créées au moyen d'images de géolocalisation directe de l'UAV RTK et de l'UAV non RTK et une série a été créée en utilisant les GCP durant l'orientation externe des images de l'UAV non RTK. La précision spatiale a été déterminée à partir des erreurs résiduelles horizontales (X,Y) et verticales (Z) et des erreurs moyennes quadratiques (EMQ) relatives aux 17 points de vérification horizontaux et aux 180 points de vérification verticaux mesurés par un

minirobot mobile et une station de base GNSS/RTK. Pour les deux jeux de données de géolocalisation directe, la précision horizontale et verticale a été substantiellement améliorée grâce aux récepteurs de précision GNSS/RTK embarqués à bord de l'UAV RTK, réduisant effectivement les valeurs de l'EMQ en X, Y et Z par des ordres de grandeur de 1 à 2 comparativement au récepteur GPS de précision inférieure embarqué à bord de l'UAV non RTK. Ce qui importe, c'est que la précision horizontale des données de l'UAV RTK traitées au moyen de la géolocalisation directe était équivalente à la précision horizontale des données de l'UAV non RTK traitées avec les GCP, mais l'erreur verticale des DSM des données de l'UAV RTK était de deux à trois fois plus importante que celle des DSM des données non RTK avec les GCP. Dans l'ensemble, les résultats suggèrent que la géolocalisation directe avec l'UAV RTK permet d'obtenir une précision horizontale comparable à celle obtenue avec un réseau de GCP, mais pour les mesures topographiques nécessitant la plus grande précision possible, les chercheurs et les praticiens devraient utiliser les GCP.

Introduction

Major advances in platforms, components, analytics and software have positioned unmanned aerial vehicles (UAVs) at the intersection of many diverse fields of science and engineering, and have driven major investment and research growth in recent years (e.g., *Hardin and Jensen* [2011]; *Hugenholtz et al.* [2012]; *Watts et al.* [2012]; *Nex and Remondino* [2013]; *Whitehead and Hugenholtz* [2014]; *Whitehead et al.* [2014]). Once dominated by military applications, UAVs are now used for mapping and surveying in a wide range of commercial and civil applications, such as agriculture, mining, environmental assessment and monitoring, construction and transportation. UAV data address a range (≈ km^2) and spatial resolution (≈ cm/pixel) gap between ground-based and conventional aerial and satellite surveying techniques and allow on-demand surveys due to their relative ease of deployment [*Hugenholtz et al.* 2013]. Consequently, global adoption of UAVs for operational mapping and surveying has increased dramatically over the past decade.

Most research and development (R&D), and operational use of UAVs for mapping and surveying has focused on small platforms (< 25 kg) as this class is generally more amenable to airspace regulations [*Hugenholtz et al.* 2012] and involves lower capital and operating costs. There are a number of important differences between manned aircraft and small UAVs for mapping and surveying: (1) UAVs are less stable during flight, which results in variable image geometry and overlap; (2) UAVs typically use compact cameras with limited and unstable calibration; and (3) UAVs fly much closer to the ground, yielding greater off-nadir distortion [*Whitehead and Hugenholtz* 2014]. Early studies involving UAV photogrammetry relied on conventional software developed for manned aircraft surveys (e.g., *Hugenholtz et al.* [2013]), which requires well-calibrated cameras and imposes rigorous constraints on image geometry to optimize accuracy. More recently, advances in structure from motion (SfM) and computer vision software have made it easier to address the geometric variability and distortion inherent in UAV images and demonstrated success in producing highly accurate orthoimages and digital surface models (DSMs) [*James and Robson* 2012; *Westoby et al.* 2012; *Fonstad et al.* 2013].

The spatial accuracy of UAV-derived DSMs and orthoimages has been examined in a number of studies (e.g., *Harwin and Lucieer* [2012]; *Hugenholtz et al.* [2013, 2015]; *Turner et al.* [2014]; *Tamminga et al.* [2015a, 2015b]; *Whitehead and Hugenholtz* [2015]). For example, using ground control points (GCPs) and conventional photogrammetry software (Trimble Inpho®) applied to UAV imagery over a grassland site, *Hugenholtz et al.* [2013] obtained root-mean-square-errors (RMSE) of 0.18 m in the horizontal (RMSER) for orthoimagery and 0.29 m in the vertical (RMSEZ) for the digital elevation modem (DEM). Using GCPs and Pix4D SfM software, *Whitehead and Hugenholtz* [2015] obtained $RMSE_R$ = 0.048 m and $RMSE_Z$ = 0.035 m along a sub-aerially-exposed gravel river channel. Errors obtained by *Whitehead and Hugenholtz* [2015] meet the newly-released accuracy standards for digital geospatial data developed by the American Society for Photogrammetry and Remote Sensing (ASPRS) at the 0.1 m RMSE level.

In cases where GCPs cannot be deployed due to safety concerns, terrain conditions or time constraints, it is still possible to produce orthoimages and DSMs without GCPs, using a technique known as direct georeferencing. This approach uses the onboard GNSS and inertial measurement unit (IMU) to determine the position and orientation of the camera. SfM software alleviates some of the orientation issues, so the main priority for UAVs is determining the position of the images, which is mainly a function of the GNSS. *Turner et al.* [2014] showed that it is possible to achieve a horizontal accuracy of 0.11 m using a single-frequency carrier-phase differential GPS (DGPS) unit onboard a small

octocopter UAV. Importantly, *Turner et al.* [2014] did not examine vertical accuracy, how accuracy changes relative to the quality of the onboard GNSS, or how the vertical accuracy of DSMs changes with or without inclusion of GCPs. These gaps are what motivated the research herein.

In this paper, we compare the accuracy of orthoimages and DSMs produced from UAV images using GCPs and direct georeferencing (i.e., without GCPs). We examined the accuracy of direct georeferencing applied to one of the first commercially-available fixed-wing UAVs that integrates a survey-grade GNSS/RTK receiver. A network of 17 horizontal check points and 180 vertical check points was used to test accuracy. Results provide direction to researchers and practitioners considering UAV mapping and surveying with or without GCPs.

Methods

The field test was performed at an active gravel quarry north of Taber, Alberta, Canada (Figure 1). The surface ranged from gravel-covered in the active quarry area, to short sparse grass (< 0.05 m) in the intact (undisturbed) gravel deposit bordering the pit. The nature of the short grass surrounding the active pit is such that we consider it as "non-vegetated," which is an important distinction in the context of examining vertical accuracy.

Two line-of-sight flights were carried out on September 29, 2015, first using an eBee fixed-wing UAV equipped with Canon S110 (12 MP) RGB camera, and then using the eBee RTK UAV and the same camera. Both UAVs are manufactured by senseFly SA (*sensefly.com*). The only significant difference between these UAVs is the more advanced GNSS (L1/L2, GPS and GLONASS) onboard the eBee RTK. A company white paper outlining the features of the eBEE RTK states that it can achieve horizontal and vertical accuracies of 0.03 m and 0.05 m, respectively [*Roze et al.* 2014]. During the eBee RTK flight, real-time position corrections from a Trimble R6 (GPS/GLONASS) base station were streamed to the UAV. Flight planning and control were performed using the same proprietary software for both flights (eMotion). Both flights involved identical north-south flight lines with 80% lateral and longitudinal overlap, yielding 287 images. Atmospheric conditions during the flights consisted of broken cloud and light winds

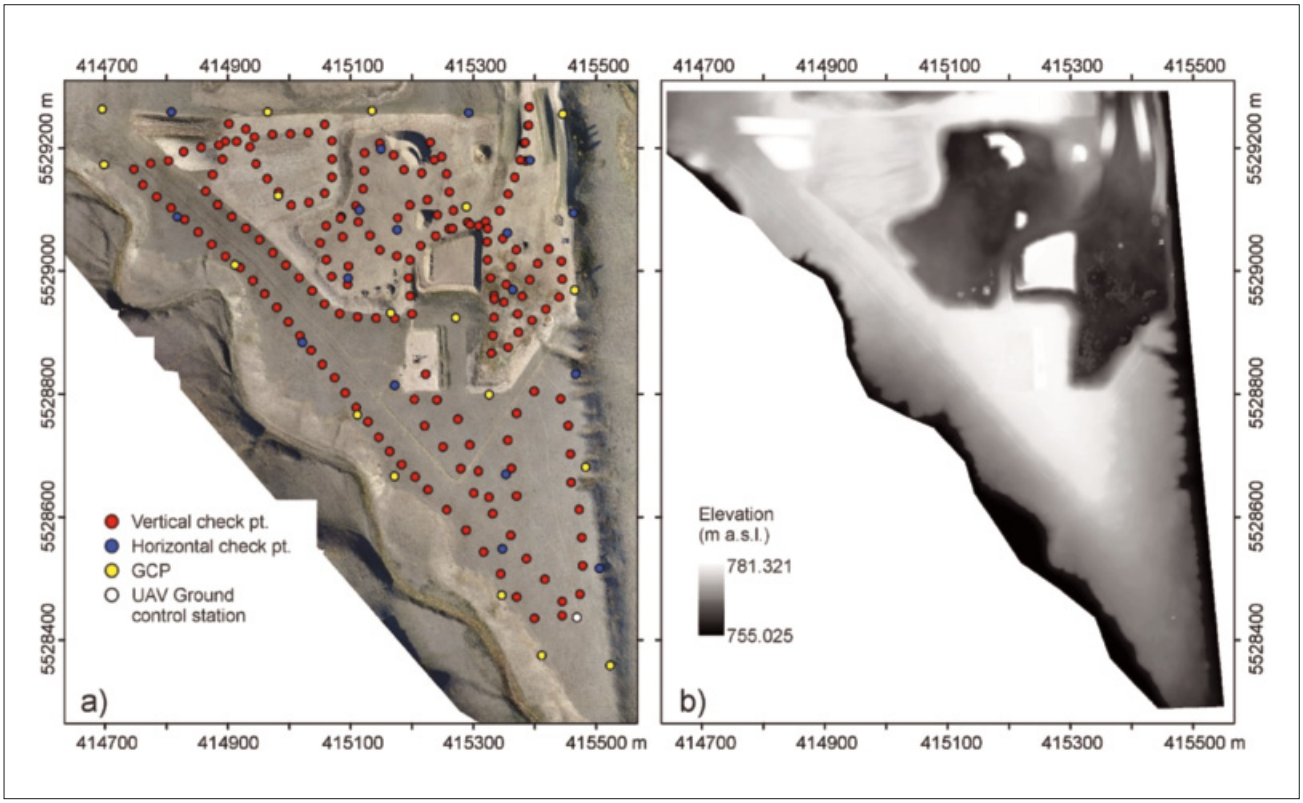

Figure 1: Overview of the study site (49.907°N, 112.181°W). The orthoimage in (a) shows the locations of vertical check points (red circles), horizontal check points (blue circles) and GCPs (yellow circles). (b) A DSM of a portion of the area in (a) showing the variation in topography between the active pit and the intact gravel deposit to the south.

(3–6 ms^{-1} at flight level). Throughout this paper we refer to the eBee RTK as the "RTK UAV" and the eBee as the "non-RTK UAV."

Postflight Terra 3D was used to process the imagery. This registered software is supplied with the eBees and is designed specifically for this application. Postflight Terra 3D incorporates *Lowe*'s [2004] scale-invariant feature transform (SIFT) algorithm to match key points across multiple images [*Küng et al.* 2011] and processes data in three key steps: (1) initial processing (camera internals and externals, automated aerial triangulation, bundle block adjustment); (2) point cloud densification; and (3) digital surface model (DSM) and orthomosaic generation. Three sets of orthoimages and DSMs were produced from the flights, including two by direct georeferencing images from the RTK UAV and non-RTK UAV and one involving GCPs during processing of the non-RTK UAV images. For the latter, 18 GCPs were used to complete the external camera orientation. DSMs were interpolated from the densified point clouds and used to orthorectify the individual images. The final step combined the orthorectified images to form a seamless orthoimage mosaic. Orthoimages and DSMs were produced at a spatial resolution of 0.052 m (Figure 1b).

Field measurements prior to the flights involved measuring the coordinates of GCPs and check points using a GNSS/RTK base station and rover. The horizontal and vertical accuracy of the field GNSS/RTK survey was < 0.010 m. GCPs and horizontal check points consisted of painted X's that were distributed throughout the study site and easily resolvable in the images. In total, 17 painted X's were used as horizontal check points to assess the planimetric accuracy of the orthoimages. An additional 180 vertical check points were recorded throughout the study site and used to assess the vertical accuracies of the DSMs. Following the protocols outlined in *ASPRS* [2015], spatial accuracy was determined from the measured offset (error or residual) between the observed (field-based GNSS/RTK measurements) and predicted (UAV data) easting (X), northing (Y) and vertical (Z) coordinates. We also calculated the root-mean-square-error (RMSE):

$$RMSE_{X,Y,Z} = \sqrt{\frac{1}{n}\sum_{i=1}^{n}\left(X,Y,Z_{i(predicted)} - X,Y,Z_{i(observed)}\right)^2} \quad (1)$$

where $X,Y,Z_{i(predicted)}$ is the coordinate (in *X*-, *Y*-, or *Z*-directions) of the i^{th} check point from the UAV data; $X,Y,Z_{i(observed)}$ is the coordinate (in *X*-, *Y*-, or *Z*-directions) of the i^{th} check point according to the field-based GNSS/RTK survey; *n* is the number of check points tested; and *i* is an integer index (range from 1 to *n*). Total horizontal error ($RMSE_R$) was calculated from:

$$RMSE_R = \sqrt{RMSE_X^{\,2} + RMSE_Y^{\,2}} \quad (2)$$

The "predicted" point data were obtained using two approaches. For horizontal accuracy, the center coordinates of the X's were sampled manually from the orthoimages, while for vertical accuracy the elevations of points in the DSMs corresponding to the locations of vertical check points were obtained using an automated sampling procedure in ArcGIS v10.2.2 software. In total, the orthoimages and DSMs produced from the UAV data encompass an area of 0.48 km^2 (48 ha; Figure 1).

Results

Kernel density plots in Figure 2 show the distributions of check point residuals (errors) between the observed (GNSS/RTK) and predicted (DSM) coordinates. With the exception of the X-error distribution from the orthoimage processed with non-RTK UAV images and GCPs, Shapiro-Wilks normality tests at the 0.01 threshold level indicate that all the distributions of check point residuals can be modelled as normal distributions. This is important because it has implications for the use of Equations 1 and 2, which require the residuals to be normally distributed (cf. *ASPRS* [2015]).

Kernel density plots of X and Y errors from the orthoimages produced by direct georeferencing images from the RTK UAV reveal uni-modal distributions with clustering around zero for the X and Y errors (Figure 2a). The $RMSE_X$ and $RMSE_Y$ were 0.023 m and 0.022 m, respectively, giving an $RMSE_R$ of 0.032 m and mean absolute errors (MAE) of 0.018 m ($\sigma = 0.021$) in X and 0.018 m ($\sigma = 0.023$) in Y. These values are very similar to those from the non-RTK UAV data processed with GCPs (Figure 2b), which yielded 0.024 m and 0.023 m for $RMSE_X$ and $RMSE_Y$, respectively, ($RMSE_R = 0.034$ m) and MAEs of 0.022 m ($\sigma = 0.025$) in X and 0.017 m ($\sigma = 0.021$) in Y. For the non-RTK UAV data processed via direct georeferencing (Figure 2c), the $RMSE_X$ and $RMSE_Y$ were 0.633 m and 0.557 m, respecitvely, giving an $RMSE_R$ of 0.843 m and MAEs of 0.628 m ($\sigma = 0.079$) in X and 0.556 m ($\sigma = 0.045$) in Y. This represents an increase in horizontal error by more than 2 orders of magnitude compared to the RTK UAV data.

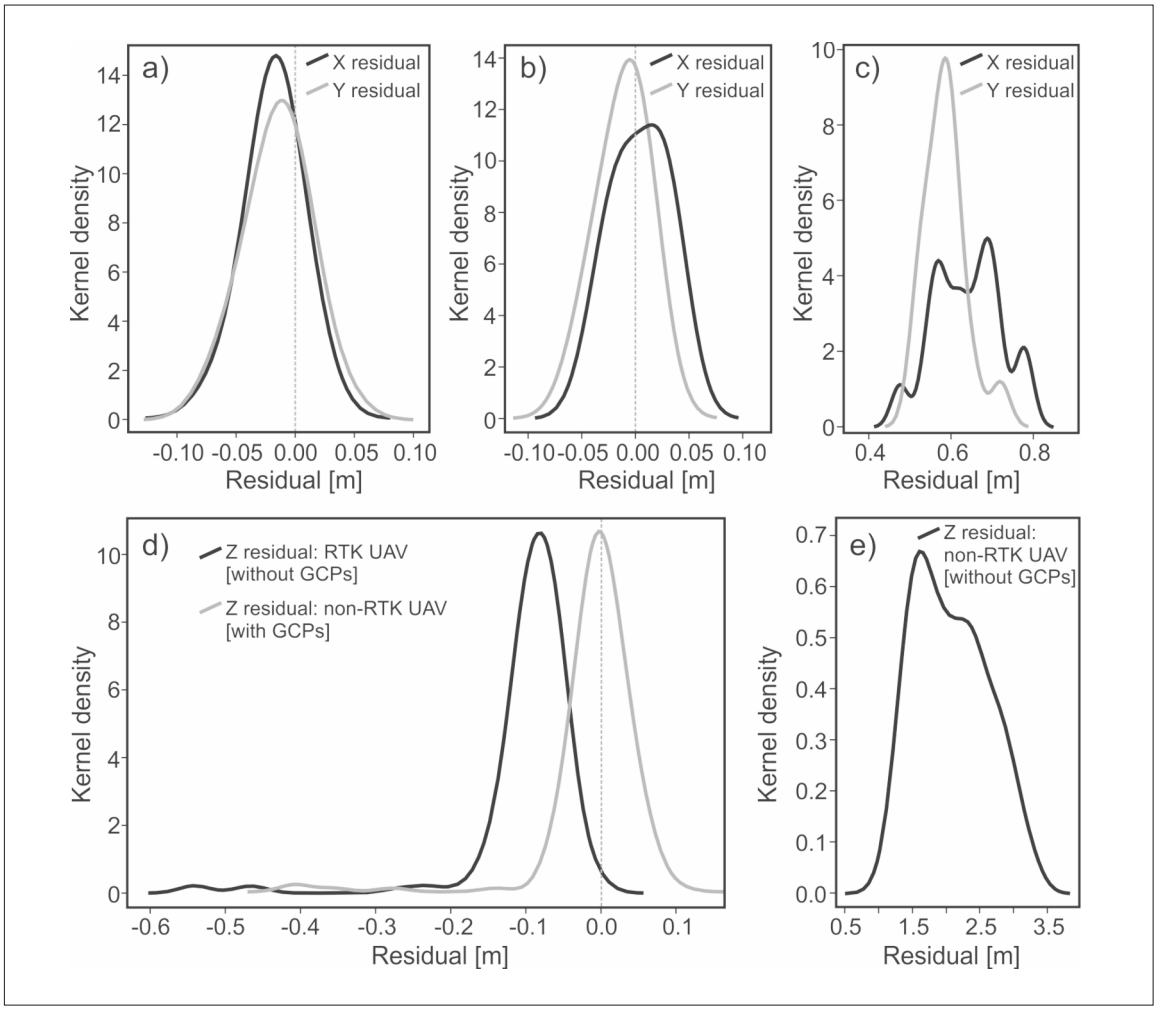

Figure 2: The top plots show the distribution of X and Y residuals for the (a) RTK UAV data processed via direct georeferencing, (b) non-RTK UAV data processes with GCPs, and (c) non-RTK UAV data processed via direct georeferencing. The lower plots show the distributions of Z residuals for (d) the RTK data processed via direct georeferencing and the non-RTK data processed with GCPs, and (e) the non-RTK UAV data processed via direct georeferencing. The plots were developed using Gaussian kernels with a 0.02 bandwidth for (a) to (d) and a 0.2 bandwidth for (e).

Kernel density plots of Z errors in the DSMs reveal uni-modal distributions (Figures 2d and 2e); however, the only Z-error distribution that clusters near 0 is from the non-RTK UAV images processed with GCPs. The Z-error distribution from the DSM produced with the RTK UAV images is shifted to the left of zero, indicating that the elevations of the vertical check points were systematically lower than the elevations of the same points predicted on the DSM, while the opposite was found in the distribution of Z error for the DSM produced with the non-RTK UAV images. A Grubbs' test [*Grubbs* 1969] revealed that the distributions in Figure 2d contained a number of outliers all located within a small area coinciding with dense weed and shrub cover. The $RMSE_Z$ values indicate that the highest accuracy was achieved in the DSM produced with GCPs and the non-RTK UAV images ($RMSE_Z = 0.063$ m; MAE = 0.032 m; $\sigma = 0.062$), while the use of direct georeferencing resulted in $RMSE_Z$ values of 0.120 m (MAE = 0.096 m; $\sigma = 0.072$) and 2.144 m (MAE = 2.076 m; $\sigma = 0.537$) in the DSMs produced with the RTK and non-RTK UAV images, respectively.

Spatial patterns of vertical error in the DSMs produced with and without GCPs are shown in Figure 3. These maps were produced by interpolating the vertical error ($E_{\text{vertical}} = Z_{i(observed)} - Z_{i(predicted)}$) of the 180 vertical check points using the spline with tension interpolator. The maps in Figures 3a and 3b show similar patterns and spatial distributions of vertical error in the DSMs for the non-RTK UAV data processed with GCPs and the RTK UAV data processed using direct

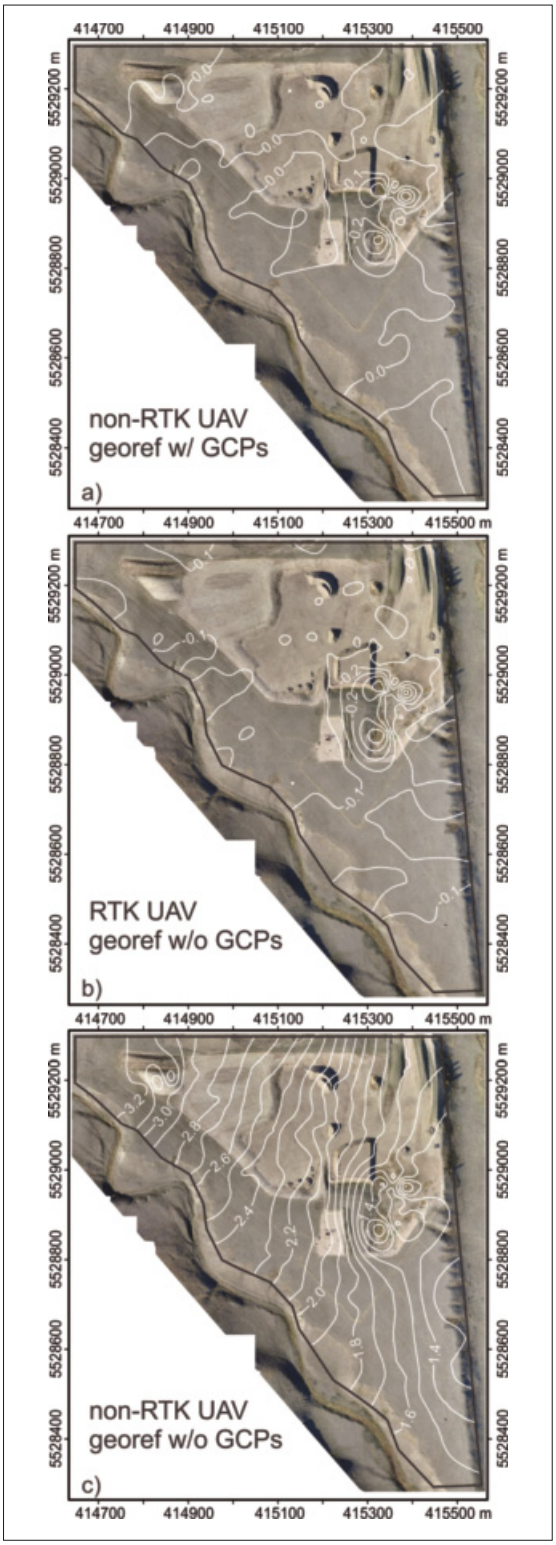

Figure 3: Maps of vertical error interpolated using spline with tension (0.1 m contour interval): (a) Z-residual map of the DSM processed with GCPs using the non-RTK UAV images; (b) Z-residual map of the DSM processed via direct georeferencing using the RTK UAV images; (c) Z-residual map of the DSM processed via direct georeferencing using the non-RTK UAV images.

georeferencing. East of the center of the study site is an area of higher vertical error, which reaches –0.563 m in the DSM from the RTK UAV data and –0.425 m in the DSM from the non-RTK UAV data processed with GCPs. The negative values indicate that the DSM elevation is higher than the elevation recorded by the check points. According to the Grubbs' test, this area also coincides with the occurrence of outliers in both datasets. Field observations during the acquisition of vertical check points suggest the reason for the increased error is due to the presence of dense vegetation, primarily in the form of small shrubs and weeds (approximately 0.2–0.5 m tall). While the check points record the ground surface elevation, the DSM records the top of the vegetation, resulting in increased error. Removing the outliers associated with vegetation improves the vertical accuracy of the DSMs produced via direct georeferencing, with the largest improvement in the DSM produced with GCPs using the non-RTK UAV data ($RMSE_Z = 0.030$ m) followed by the DSM produced via direct georeferencing using the RTK UAV data ($RMSE_Z = 0.089$ m).

The pattern of elevated error coinciding with vegetation also occurs in the error map for the DSM produced by direct georeferencing using the non-RTK UAV data, but there are other artifacts in Figure 3c that indicate some striking differences with the other datasets. In particular, there is a systematic increase in vertical error towards the northwest portion of the study site, which is a common effect caused by boresight misalignment (the angular misalignment between the GPS/IMU and the camera). Currently the only way to resolve this effect is to use GCPs or a higher quality GNSS onboard the UAV.

Discussion

This investigation examined the spatial accuracy of orthoimages and DSMs produced from UAV images processed with and without GCPs. We also tested the accuracy of one of the first commercially-available, fixed-wing RTK UAVs (eBee RTK, Sensefly SA). By isolating the GNSS as the only difference between UAV platforms, our results show that the horizontal and vertical accuracy of the DSMs and orthoimagery depends mainly on the quality of the GNSS onboard the UAV and whether GCPs are used in the processing. Comparison of two DSMs and orthoimages processed via direct georeferencing revealed that the use of a survey-grade GNSS onboard the UAV improved the horizontal

and vertical accuracy by 1 to 2 orders of magnitude. The horizontal accuracy of orthoimagery produced via direct georeferencing the RTK UAV images was very similar to the accuracy obtained with the non-RTK UAV images using GCPs; however, the vertical accuracy of the DSMs differed by a factor of 1.9, with the latter yielding a lower $RMSE_Z$.

The MAEs in X and Y obtained from the orthoimage produced with the RTK UAV data are an improvement from those reported in a study involving direct georeferencing applied to image data from an octocopter with a customized DGPS [*Turner et al.* 2014]. The RMSE values for X and Y are also an improvement from those reported by *Whitehead and Hugenholtz* [2015] using GCPs and non-RTK UAV data. In the context of the new ASPRS digital mapping standards [*ASPRS* 2015], our results indicate that direct georeferencing of imagery from the RTK UAV can fulfill the requirements for horizontal mapping at the 0.025 m horizontal accuracy class for $RMSE_X$ and $RMSE_Y$. The same class applies to the non-RTK UAV data processed with GCPs. This is equivalent to Class 1 accuracy at the 1:100 map scale under the ASPRS accuracy standards for large-scale maps [*ASPRS* 1990] (Table 1). In contrast, direct georeferencing with non-RTK UAV data fulfills the requirements for horizontal mapping at the 0.600 m horizontal accuracy class for $RMSE_X$ and $RMSE_Y$, which is equivalent to Class 1 accuracy at the 1:2400 map scale under *ASPRS* [1990]. For applications that cannot incorporate GCPs, the results suggest practitioners can achieve a significant improvement in horizontal accuracy using an RTK UAV.

The vertical accuracy of the DSMs produced with and without GCPs shows a broad range. The application of direct georeferencing to the non-RTK UAV data yielded an $RMSE_Z$ of 2.144 m and a well-defined drift in vertical accuracy over the study area, likely caused by boresight misalignment. This suggests that UAVs equipped with consumer-grade GPSs (without post-processing) are unsuitable for survey-grade topographic measurements unless GCPs are incorporated into the processing workflow. In contrast, the DSM processed from the RTK UAV data using direct georeferencing produced a much lower $RMSE_Z$ (0.120 m), which shows that a considerable improvement can be achieved by integrating a survey-grade GNSS/RTK receiver. Using GCPs achieves the highest vertical accuracy, with an $RMSE_Z$ comparable to other studies involving the same platform. Removal of check points from densely vegetated areas at the study site further improved the $RMSE_Z$ values for DSMs produced with GCPs using the non-RTK data ($RMSE_Z$ = 0.030 m) and via direct georeferencing using RTK UAV data ($RMSE_Z$ = 0.089 m). The former $RMSE_Z$ value is one of the lowest reported in the literature to date. Thus, to optimize the vertical accuracy of DSMs, researchers and practitioners should use GCPs. However, for applications in which an $RMSE_Z \approx 0.120$ m is acceptable, direct georeferencing with images from an RTK UAV platform can avoid the time-consuming process of deploying and measuring GCPs and is still an improvement over LiDAR collected by manned aircraft {Missing in reference list}[*Hodgson and Bresnahan* 2004] in areas with little to no vegetation. According to *ASPRS* [2015], the DSM produced by direct georeferencing the RTK UAV images is in the 0.100 m non-vegetated vertical accuracy class, which is equivalent to the 0.300 m Class 1 contour interval per *ASPRS* [1990], whereas the DSM produced with GCPs is in the 0.050 m non-vegetated vertical accuracy class, which is equivalent to the 0.150 m Class 1 contour interval per *ASPRS* [1990].

There are a number of practical implications associated with the higher vertical error in the DSM

Table 1: Overview of spatial errors of each dataset and associated *ASPRS* [2015] accuracy classes.

Dataset	$RMSE_X$ (m)	$RMSE_Y$ (m)	$RMSE_R$ (m)	Non-vegetated $RMSE_Z$ (m)	ASPRS (2015) Horizontal Accuracy Class $RMSE_x$ and $RMSE_y$ (m)	ASPRS (2015) Vertical Accuracy Class (m)	Equivalent Class 1 contour interval per ASPRS 1990 (m)	Equivalent Class 2 contour interval per ASPRS 1990 (m)
Non-RTK UAV w/ GCPs	0.024	0.023	0.034	0.030	0.025	0.050	0.150	0.075
Non-RTK UAV w/o GCPs	0.633	0.557	0.843	2.144	0.600	3.333	9.999	5.000
RTK UAV w/o GCPs	0.023	0.022	0.032	0.089	0.025	0.100	0.300	0.150

produced by direct georeferencing using the RTK UAV data. For example, the error in individual DSMs propagates into differencing (i.e., DSM of difference, DoD), which has implications for the accuracy of measurements involving volumetric changes associated with erosion and deposition, excavation and stockpiling (e.g., earthworks, mining) and deformation (e.g., landslides, structures). We can define a critical level of detection (LoD) to account for error:

$$LoD = \pm 3 \times \sqrt{\left(RMSE_{Z1}\right)^2 + \left(RMSE_{Z2}\right)^2} \qquad (3)$$

where $RMSE_{Z1}$ is for the first DSM and $RMSE_{Z2}$ is for the second DSM, and the multiplier, 3, represents the extreme tails of a normal probability distribution (cf. *Hugenholtz et al.* [2013]). If the non-vegetated $RMSE_Z$ values are used for the two DSMs with the highest vertical accuracy and assume equivalent $RMSE_Z$ values in subsequent DSMs produced using the same methods, the estimated LoDs are 0.378 m for the RTK UAV data processed via direct georeferencing and 0.127 m for the non-RTK UAV data processed with GCPs. Any vertical difference in the DoD that is smaller than these values cannot be deemed as real. The ability to resolve and quantify volumetric change becomes increasingly difficult with higher vertical error. For some applications, the $RMSE_Z$ of the DSM produced by direct georeferencing the RTK UAV will be too high to reliably detect change. To reduce error and its propagation into DoDs, our results recommend that researchers and practitioners should use GCPs if analyses with multi-temporal topographic data are required.

One of the indirect outcomes of this investigation is that our tests were able to reproduce the 0.03 m horizontal accuracy ($RMSE_R$) reported by the manufacturer of the RTK UAV, although we were not able to reproduce vertical accuracy (0.05 m) reported in their white paper [*Roze et al.* 2014]. Several factors could account for this discrepancy. For example, 180 vertical check points distributed across the survey area were used, whereas *Roze et al.* [2014] only utilized 19. Furthermore, compared to our site, the test site reported by *Roze et al.* [2014] was relatively flat and does not appear to contain any significant slopes or changes in relief. This may be the most important difference leading to the higher vertical error in our case study. The results also indicate that wind speed can increase the error, which may have been a small factor in our case study.

Conclusions

We tested the spatial accuracy of orthoimages and DSMs processed with and without GCPs using images acquired by two commercially-available fixed-wing UAVs. Two aerial surveys were conducted over an active gravel pit, first using the non-RTK UAV equipped with a consumer-grade GPS, and then using the RTK UAV equipped with a survey-grade GNSS/RTK (L1/L2, GPS and GLONASS). These data were processed with and without GCPs to yield three orthoimages and DSMs. The $RMSE_R$ of the orthoimages produced with images from the RTK UAV and non-RTK UAV were virtually identical. Our results support the UAV vendor's claim of a 0.03-m horizontal accuracy; however, we were not able to reproduce the 0.05-m vertical accuracy they obtained [*Roze et al.* 2014]. The $RMSE_Z$ of the direct georeferenced RTK UAV data was 0.120 m, which is a major improvement from the $RMSE_Z$ obtained with the non-RTK UAV data (2.144 m), but almost double the $RMSE_Z$ from the non-RTK UAV data processed with GCPs (0.063 m). The $RMSE_Z$ value decreased by a factor of 2 for the DSM produced with GCPs using the non-RTK UAV images, but only by a factor of 1.3 for the DSM produced with direct georeferencing using the RTK UAV images. Collectively, our results can inform researchers and practitioners considering the accuracy of an RTK UAV for mapping and surveying. Direct georeferencing with the RTK UAV data is appropriate for projects requiring the highest horizontal accuracy thresholds, but for the highest achievable vertical accuracy thresholds, practitioners should use GCPs.

Acknowledgements

The authors acknowledge field assistance from Jamin Doherty.

MS rec'd 02/11/15
Revised MS rec'd 29/01/16

References

American Society for Photogrammetric Engineering and Remote Sensing (ASPRS). 1990. Accuracy standards for large-scale maps. *Photogrammetric Engineering and Remote Sensing.* 56(7): 1068–1070.

American Society for Photogrammetric Engineering and Remote Sensing (ASPRS). 2015. ASPRS positional accuracy standards for digital geospatial data

(Edition 1, Version 1.0., November, 2014). *Photogrammetric Engineering & Remote Sensing*. 81(3): A1–A26.

Fonstad, M.A., J.T. Dietrich, B.C. Courville, J.L. Jensen and P.E. Carbonneau. 2013. Topographic structure from motion: a new development in photogrammetric measurement. *Earth Surface Processes and Landforms*. 38(4): 421–430.

Grubbs, F.E. 1969. Procedures for detecting outlying observations in samples. *Technometrics*. 11: 1–21 .

Hardin, P.J., and R.R. Jensen. 2011. Small-scale unmanned aerial vehicles in environmental remote sensing: challenges and opportunities. *GIScience & Remote Sensing*. 48(1): 99–111.

Harwin, S., and A. Lucieer. 2012. Assessing the accuracy of georeferenced point clouds produced via multi-view stereopsis from unmanned aerial vehicle (UAV) imagery. *Remote Sensing*. 4(6): 1573–1599.

Hodgson and Bresnahan 2004 -- needs reference

Hugenholtz, C.H., B.J. Moorman, K. Riddell and K. Whitehead. 2012. Small unmanned aircraft systems for remote sensing and Earth science research. *EOS*. 93(25): 236–237.

Hugenholtz, C.H., K. Whitehead, O.W. Brown, T.E. Barchyn, B.J. Moorman, A.J. LeClair, K. Riddell and T. Hamilton. 2013. Geomorphological mapping with a small unmanned aircraft system (sUAS): feature detection and accuracy assessment of a photogrammetrically-derived digital terrain model. *Geomorphology*. 194: 16–24.

Hugenholtz, C.H., J. Walker, O.W. Brown and S. Myshak. 2015. Earthwork volumetrics with an unmanned aerial vehicle and softcopy photogrammetry. *Journal of Survey Engineering*. 141(1): 06014003.

James, M.R., and S. Robson. 2012. Straightforward reconstruction of 3D surfaces and topography with a camera: Accuracy and geoscience application. *Journal of Geophysical Research—Earth Surface*. 117(F3): F03017.

Küng, O., C. Streecha, A. Beyeler, J.-C. Zufferey, D. Floreano, P. Fua and F. Gervaix. 2011. The accuracy of automatic photogrammetric techniques on ultra-light UAV imagery. *International Archives of the Photogrammetry, Remote Sensing and Spatial Information Sciences*, Volume XXXVIII-1/C22, 2011 ISPRS Zurich 2011 Workshop, 14–16 September 2011, Zurich, Switzerland. 125–130.

Lowe, D.G. 2004. Distinctive image features from scale-invariant keypoints. *International Journal of Computer Vision.* 60(2): 91–110.

Roze, A., J.-C. Zufferey, A. Beyeler and A. McClellan. 2014. eBee RTK accuracy assessment. Sensefly White Paper, 7p [https://www.sensefly.com/fileadmin/user_ upload/sensefly/ documents/eBee-RTK-Accuracy-Assessment.pdf].

Tamminga, A., C.H. Hugenholtz, B. Eaton and M. Lapointe. 2015a. Hyperspatial remote sensing of channel reach morphology and hydraulic fish habitat using an unmanned aerial vehicle (UAV): a first assessment in the context of river research and management. *River Research and Applications*. 31(3): 379–391.

Tamminga, A., B. Eaton and C.H. Hugenholtz. 2015b. UAS-based remote sensing of fluvial change following an extreme flood event. *Earth Surface Processes and Landforms*. 40(11): 1464–1476.

Turner, D., A. Lucieer and L. Wallace. 2014. Direct georeferencing of ultrahigh-resolution UAV imagery. *IEEE Transactions on Geoscience and Remote Sensing*. 52(5: 2738–2745.

Nex, F. and F. Remondino. 2013. UAV for 3D mapping applications: a review. *Applied Geomatics*. 6(1): 1–15.

Watts, A.C., V.G. Ambrosia and E.A. Hinkley. 2012. Unmanned aircraft systems in remote sensing and scientific research: classification and considerations of use. *Sensors.* 4(6): 1671–1692.

Westoby, M.J., J. Brasington, N.F. Glasser, M.J. Hambrey and J.M. Reynolds. 2012. 'Structure-from-Motion' photogrammetry: a low-cost, effective tool for geoscience applications. *Geomorphology*. 179: 300–314.

Whitehead, K., and C.H. Hugenholtz. 2014. Remote sensing of the environment with small unmanned aircraft systems (UASs), part 1: a review of progress and challenges. *Journal of Unmanned Vehicle Systems*. 2(3): 69–85.

Whitehead, K., C.H. Hugenholtz, S. Myshak, O.W. Brown, A.J. LeClair, A. Tamminga, T.E. Barchyn, B.J. Moorman and B. Eaton. 2014. Remote sensing of the environment with small unmanned aircraft systems (UASs), part 2: scientific and commercial applications. *Journal of Unmanned Vehicle Systems*. 2(3): 86–102.

Whitehead, K., and C.H. Hugenholtz. 2015. Applying ASPRS accuracy standards to surveys from small unmanned aircraft systems (UAS). *Photogrammetric Engineering and Remote Sensing*. 81(10): 787–793.

Authors

Chris Hugenholtz[1] *chhugenh@ucalgary.ca*
Owen Brown[2] *owen.brown@ventusgeo.com*
Jordan Walker[2] *jordan.walker@ventusgeo.com*
Thomas Barchyn[1] *tbarchyn@gmail.com*
Paul Nesbit[1] *prnesbit@gmail.com*
Maja Kucharczyk[1] *maja.kucharczyk@ucalgary.ca*
Steve Myshak[2] *steve.myshak@ventusgeo.com*

[1]Department of Geography, University of Calgary Calgary, Alberta, Canada

[2]Ventus Geospatial, Lethbridge, Alberta, Canada ❑